DOI:10.1021/jf9040904

JOURNAL OF AGRICULTURAL AND FOOD CHEMISTRY
ARTICLE

Study of the Physical Properties of Whey Protein Isolate and Gelatin Composite Films

Yanfeng Jiang, Yanxia Li, Zhi Chai, and Xiaojing Leng*

CAU & ACC Joint-Laboratory of Space Food, Key Laboratory of Functional Dairy Science of Beijing and Ministry of Education, College of Food Science & Nutritional Engineering, China Agricultural University, No. 17 Qinghua East Road, Haidian, Beijing 100083, China

The relationships between the microstructural and physical properties of the whey protein isolate and gelatin (WPI/gelatin) composite films were investigated in the present work. Through the electrostatic effects at pH 8, WPI and gelatin molecules could form compact aggregates in solution, where a remarkable shrinkage of the gelatin molecules was observed, when the WPI/gelatin mass ratio was close to 50W:50G. FT-IR analysis indicated that hydrogen bonding also involved the aggregation and film-forming process. The melting temperature of the 50W:50G composite film increased by 9 °C compared with the single component films. However, this aggregation process also made the film network microstructure discontinuous, and led to a decline of the puncture strength of the film near 50W:50G; in contrast, the deformation and water vapor permeability of the composite films increased with the gelatin content, while the moisture content and solubility did not show significant variations.

KEYWORDS: Gelatin; whey protein isolate; edible film; aggregation; shrinkage

INTRODUCTION

In recent years, edible films and coating materials are more and more used for food packaging to improve the food quality by serving as mass transfer barriers between food components and the surrounding systems. Many biomacromolecules including proteins, carbohydrates and lipids have been used for different purposes (*1*−*4*). Lipid based films have proved to be good water vapor barriers (*5*−*7*). Protein and carbohydrate based films have good tensile properties, and protein/protein or carbohydrate composite films have more controllable physical properties (*8*−*13*).

The physical properties of the composite films depend upon the nature of the raw materials and other processing factors such as concentration, mix ratio, pH, temperature, ionic strength etc. Longares et al. (*8*) studied the sodium caseinate (NaCas)/whey protein isolate (WPI) films, and denoted that the film solubility increased with the glycerol (gly) content in the system, but could not find the variations of the tensile strength (TS) and water vapor permeability (WVP) versus NaCas/WPI mix ratio. Pérez-Gago and Krochta (*14*) studied the WPI/beeswax emulsion film, and reported that the solubility varied with pH of the system, and a high WVP could be observed at the isoelectric point, where protein aggregation lowered lipid mobility and reduced interconnectivity among lipid droplets. Simelane and Ustunol (*15*) studied WPI/collagen films, and found that the TS and the elongation (*E*) of the single WPI and collagen films did not change with a multistage cooking process, but those of the composite films were initially lower than those of the collagen films and then continued to decline during the heating stages. Wang et al. (*10*) denoted in their work that the physical properties (TS, *E*, WVP etc) of WPI/corn oil composite films were not single factor-dependent, but had complex relationships with the experimental conditions such as pH and WPI/oil mix ratio etc.

The above literature indicated that the variations of the physical properties of the films were closely related to the changes of the network microstructure; however, more deeply describing these relationships needed more details at the molecular level, and this point was the focus of the present work, where a WPI/gelatin composite system was used as a model system, and the main research methods included light scattering spectroscopy (Nanozetasizer), infrared spectroscopy (FT-IR) and electron microscopy (SEM). The reasons why WPI and gelatin were chosen in this work involved three aspects: (1) WP film was famous for its remarkable transparency, flexibility and excellent nutritional and functional properties, and therefore it became one of the most applied potential raw materials in food production (*16*−*18*); and gelatin was a worldwide mass-produced material used in the manufacture of edible biodegradable films (*12*, *19*−*22*); (2) edible packaging film is also a food, therefore it needs not only convenient mechanical properties but also a better chewing texture. The mechanical properties (for example, puncture strength) of the WPI and gelatin are very different, and thus the control of their composite system may be helpful to control the mechanical strength and chewing texture of the product; (3) although there were many reports about WPI and gelatin, the analysis about the network microstructure of the relevant composite films was still not sufficiently clear.

MATERIALS AND METHODS

Materials. Whey protein isolates (WPI, 97% w/w protein) were purchased from Davisco Foods International (Eden Prairie, MN). Gelatin (type B, pig skin) was purchased from Xia Men Hua Xuan Gelatin Co.,

*Corresponding author. Tel: + 86-10-6273-7761. Fax: + 86-10-6273-6344. E-mail: Xiaojing.leng@gmail.com.

 Published on Web 03/31/2010

Ltd. (Xia Men, China). NaOH and glycerin were both analytical grades and purchased from Beijing Chemical Factory.

Sample Preparations. WPI and gelatin solutions of different concentrations (2.5, 5, 7.5 and 10%, w/w) were prepared as follows. WPI powder was dissolved in deionized water and stirred for about 2 h until completely dissolved. Then the pH of the solutions was adjusted to 8.0 using 1 N NaOH, and they were heated in a water bath with agitation at 80 °C for 30 min. Gelatin was hydrated at room temperature for 30 min and then dissolved in 55 °C water bath with mechanical stirring for about 15 min until completely dissolved. Then the pH was adjusted to 8.0 using 1 N NaOH.

Composite film-forming solutions of 10% total protein were prepared by mixing different masses of the above two solutions with the desired ratios (100W:0G, 75W:25G, 50W:50G, 25W:75G and 0W:100G) of WPI to gelatin along with the addition of 0.4 g of glycerin/g of protein. The solutions were stirred at room temperature and then treated ultrasonically for about 10 min to remove air bubbles. Five grams of each film-forming solution was poured on Plexiglas plates (8.0×8.0 cm) and then dried at 22 ± 3 °C and 56 ± 8% relative humidity in a constant temperature and humidity chamber (Ning-bo-dong-nan-yi-qi Co., Ningbo, China). The dry films were equilibrated at 22 ± 3 °C and 56 ± 8% relative humidity for at least 48 h before being subsequently peeled from the casting surface for characterization analyses including a mechanical test and FT-IR measurements.

Zeta Potential and Particle Size. The zeta potential and particle size of single solutions or film-forming solutions measurements were carried out with a Delsa-Nano particle analyzer (Beckman Coulter Inc., Brea. CA).

Scanning Electron Microscopy (SEM). Films were mounted on aluminum stubs using high-purity silver paste and carbon paint. The surface morphology and the cross section of the films were examined by means of scanning electron microscopy (high resolution cold emission scanning electron microscope Hituchi S-5500, Japan). All samples were examined using an accelerating beam at a voltage of 5 kV.

Film Thickness. Film thickness was determined using a digital micrometer (Cheng-du-cheng-liang Co., China). For each film, the values obtained at sixteen different locations were averaged.

Mechanical Properties. A texture analyzer (TMS-Pro, Food Technology Corporation, Sterling, VA) equipped with a cylinder tip was used to determine the mechanical properties of the films. All the measurements were carried out using a load cell of 10 kg, and the analysis was performed using software provided with the texture analyzer (Texture Lab Pro Version 1.13-002, Food Technology Corporation). Each test was repeated at least five times. The film samples were placed in the middle of two polymethacrylate plates (custom-made) with a hole of 3.2 cm in diameter, and the holder was fixed with four screws. The speed of the cylindrical probe (2 mm in diameter) was 1 mm/s. Strength and deformation values at the puncture point indicated hardness and deformation capacity of the films. In order to avoid any thickness variation, the puncture strength values were divided by the thickness of the films (*23*). Puncture strength (PS, N/mm) and puncture deformation (PD, mm) were calculated from the stress−strain curves.

$$PS = \frac{FP}{L} \quad (1)$$

where FP is the max puncture strength (N); L is the thickness of the films (mm); PD is the fall distance of the probe when the films were punctured.

Moisture Content. Moisture content (MC) was determined by drying small filmstrips in an oven at 105 °C for 24 h. The weights before and after the oven drying were recorded. Moisture content was calculated as the percentage of weight loss based on the original weight. Triplicate measurements of moisture content were conducted for each type of film, and the average was taken as the result (*24*).

Water Solubility. Film solubility (S) was determined in triplicate according to the modified method proposed by Gontard, Guilbert, and Cuq (*25*). Three pieces of each film (8 cm in diameter, about 0.6 g total) were dried in an oven (105 ± 2 °C; 24 h) to obtain initial dry matter weight of the films. The dried films were weighted (m_1) and then immersed into 50 mL of distilled water for 24 h at 22 ± 1 °C. After 24 h, the unsolubilized films were taken out of the water and dried (105 ± 2 °C; 24 h) to determine the weights of the dry matter (m_2) which were not dissolved in water. The weight of dry matter dissolved was calculated as shown in eq 2 and reported as percent water solubility of the films:

$$S\,(\%) = (m_1 - m_2) \times 100/m_1 \quad (2)$$

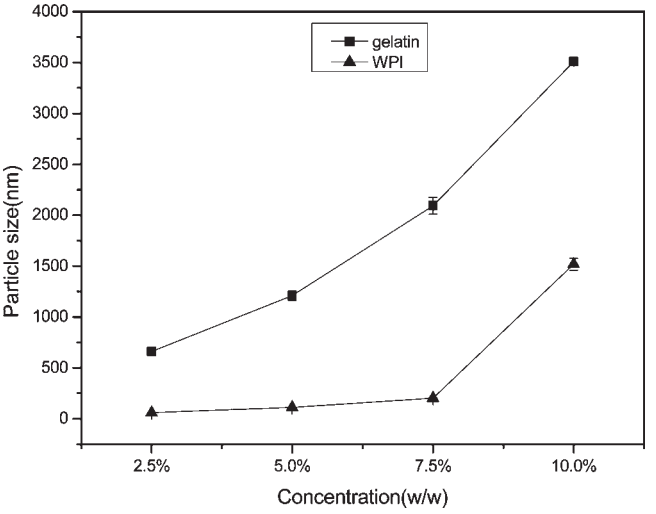

Figure 1. Size measurements of single WPI or gelatin system versus the corresponding concentrations using light scattering method. Measurements performed at room temperature and at pH 8.

Water Vapor Permeability Measurements. Water vapor permeability (WVP) of films was measured using a modified method described by Sobral et al. (*26*). Films were sealed onto a polymethyl methacrylate cup containing silica gel (0% RH), and the cups placed in a constant temperature and humidity chamber (Ning-bo-dong-nan-yi-qi Co., China) at 22 ± 1 °C and 90 ± 5% RH. The cups were weighed every hour for 6 h. Three samples in total were determined for each film type. Water vapor permeability was calculated from the equation

$$WVP = \omega x t^{-1} \cdot A^{-1} \cdot \Delta p^{-1} \quad (3)$$

where ω is the weight gain (kg), x is the film thickness (m), t is the time of gain (s), A is the permeation area (1.96×10^{-3} m^2) and Δp is the water vapor pressure differential across the film. Results were expressed as kg·s^{-1}·m^{-1}·Pa^{-1}.

Light Transmittance. The light-barrier properties of films were determined by measuring their light absorption at wavelengths ranging from 200 to 800 nm, using a UVmini-1240 spectrophotometer (Shimadzu, Kyoto, Japan). The film specimen was cut into a rectangle piece and placed in a spectrophotometer test cell directly, and air was used as reference (*27*).

Differential Scanning Calorimeter (DSC). Samples of the blended films were analyzed by differential scanning calorimeter (DSC-60, Shimadzu, Kyoto, Japan) to determine the glass transition temperatures and thermal transition temperatures. The instrument was calibrated using single indium (melting point 156.4 °C). 5−6 mg of sample was weighed and sealed in an aluminum sample pan using an encapsulating press. Duplicate samples were heated from −100 to 250 °C at a rate of 10 °C/min. An empty sample pan was used as a reference. The melting temperature was determined as the maximum temperature of the endothermic peak. The values of the endothermic enthalpy (J/g sample) were also recorded.

Fourier Transform Infrared Spectroscopy (FT-IR). All spectra were obtained using a Spectrometer GX FT-IR with a DTGS detector (Perkin-Elmer, Fremont, CA) infrared spectrophotometer over a range of 4000−400 cm^{-1} with a resolution of 4 cm^{-1}. Deconvolution of the spectra was performed using Spectrum v5.0.1.

Statistical Analyses. Statistical data were analyzed using Origin 8.0 and SPSS 16.0. Statistics on a completely randomized design were performed using the General Linear Models procedure with the one-way analyses of variance (ANOVA). Duncan's multiple range test ($P < 0.05$) was used to detect the differences among the mean values of the film properties.

RESULTS AND DISCUSSION

Zeta Potential and Particle Size of Single Components. Figure 1 compared the size variation of the single WPI and gelatin systems versus protein concentrations at pH 8. When protein concentrations

increased from 2.5 to 10%, WPI particle size increased from 60.8 ± 1.0 to 1517.7 ± 58.9 nm and gelatin from 661.5 ± 13.0 to 3507.3 ± 25.0 nm. Generally, WPI particle sizes were smaller than gelatin, and we also observed that gelatin particle size increased faster than WPI. **Figure 2** compared the variation of the zeta potential of the single WPI and the gelatin systems versus protein concentrations at pH 8. When protein concentrations increased from 2.5 to 10%, WPI zeta potential decreased from −28.6 to −18.5 mV and gelatin from −6.9 to −2.6 mV. Generally, WPI values were more negative than gelatin.

It was well reported that the increase in particle size was due to the protein flocculation caused by the disulfide linkages, intermolecular hydrogen bonds and van der Waals attractive force (*28*). Compared with gelatin, WPI particle sizes were smaller, because these proteins loaded more negative charges and the electrostatic repulsions between the molecules were thus stronger (**Figure 2**). This state hampered the flocculation process. It should also be noted that the increase in particle size could lead to a decline of the specific surface area of the particles. Taking into account the number of the ionized groups on particle surface proportional to the specific surface area, the increase in particle size could lead to a decline of the surface charge and the potential as seen in **Figure 2**. Meanwhile, it should be noted that the formation of the flocs was able to seriously change the hydrodynamic properties of the particles hence changing the measurement of the zeta potentials, i.e. in the present experimental conditions, the larger the flocs were, the lower the zeta potential was.

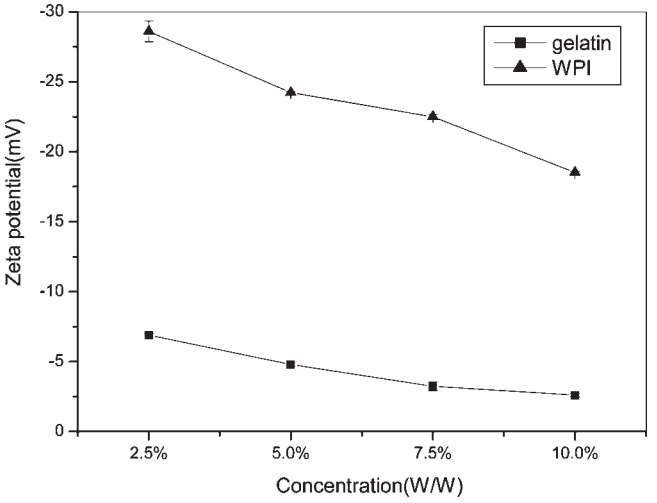

Figure 2. Zeta potential measurements of single WPI or gelatin system versus the corresponding concentrations using light scattering method. Measurements performed at room temperature and at pH 8.

Zeta Potential and Particle Size of Composite Film-Forming Solutions. Figure 3 illustrates the variation of the particle sizes and zeta potentials versus WPI/gelatin mass ratio in the film-forming solutions. When the mass ratio varied from 100W:0G to 50W:50G, the size decreased and reached a minimum value, 556.5 ± 15.4 nm, at 50W:50G. When the mass ratio continued to vary from 50W:50G to 0W:100G, the size increased up to the gelatin level. Meanwhile, the zeta potential of the composite system monotonically decreased from −18.5 to −2.6 mV when the mass ratio varied from 100W:0G to 0W:100G.

From 75W:25G to 25W:75G, the composite size increased by 35%; at 75W:25G, the composite size was 3-fold higher than that of 7.5% WPI alone, but of the same order as that of 2.5% gelatin alone; at 50W:50G, the composite size was 5-fold higher than 5% WPI alone, but 2.2-fold lower than 5% gelatin alone; at 25W:75G, the composite size was 14-fold higher than 2.5% WPI alone, but 2.4-fold lower than 7.5% gelatin alone (**Figure 1** and **3**). The above data indicated that, during the aggregation process, gelatin particles exhibited a remarkable shrinkage when the gelatin concentration was higher than 2.5%. The downward trend of the zeta potential indicated that a charge-neutralization occurred between WPI and gelatin molecules (**Figure 2**), and thus the gelatin shrinkage could be attributed to the electrostatic attractions between the negative charge in WPI matrix and the residue positive charges in gelatin matrix. The decrease of the zeta potential with the mass ratio was more complex. As discussed above, the determination of the zeta potential could be modified by the hydrodynamic properties of the flocs, which could be affected by their conformation, structure and density etc. Similarly to the single WPI and gelatin system, the increase of the size led to the decline of the zeta potential. However, the abnormal variation of the zeta potential during the shrinkage stage (from 75W:25G to 25W:75G) was not clear. Probably, the increase of the density caused by the shrinkage led

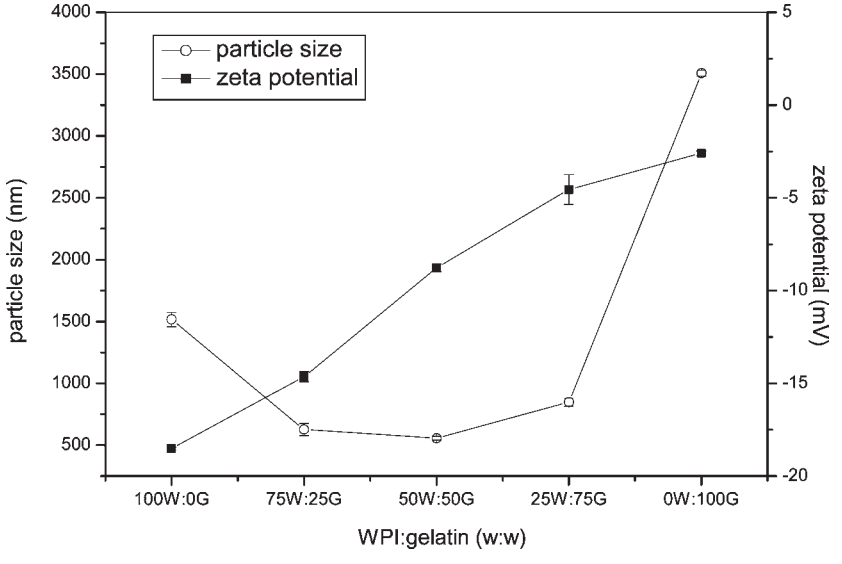

Figure 3. The measurements of zeta potential and particle size of the film-forming solutions versus WPI/gelatin mass ratios. Measurements performed at room temperature and at pH 8.

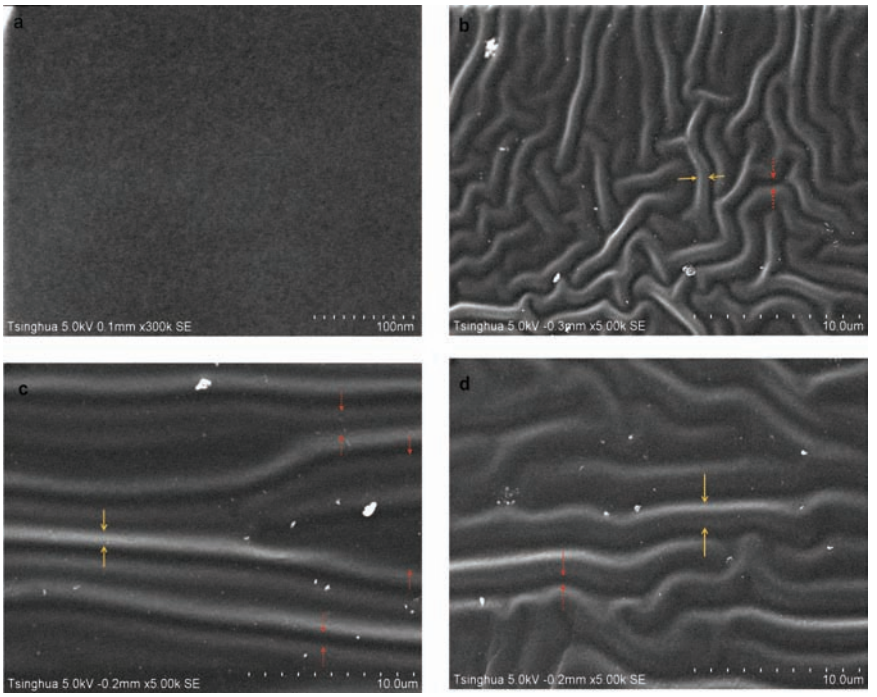

Figure 4. SEM micrographs of the surface morphology and cross sections of the films. (**a**) Surface morphology, 50W:50G. (**b**−**d**) Cross sections: **b**, 100W:0G; **c**, 0W:100G; **d**, 50W:50G.

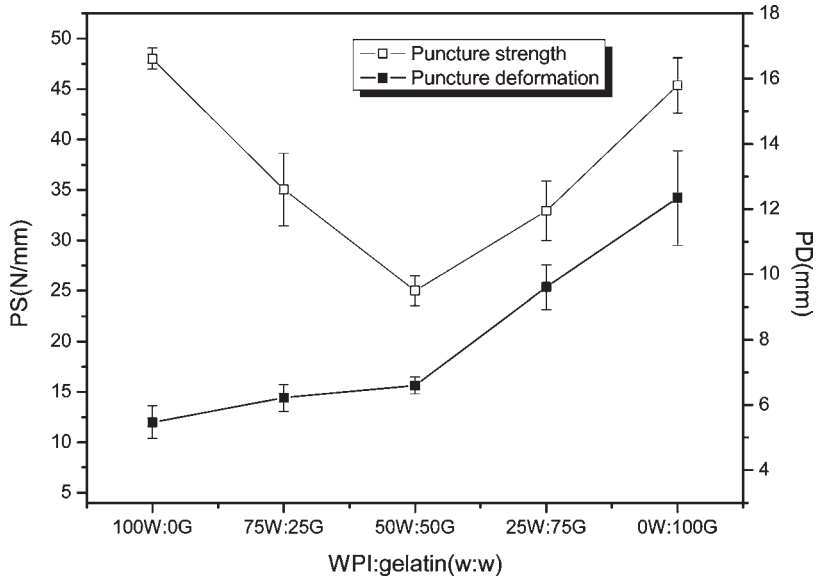

Figure 5. Mechanical properties (PS, puncture strength; PD, puncture deformation) of the films versus WPI/gelatin mass ratios.

to a settlement trend of the flocs, which modified the results of the zeta potential measurement.

Scanning Electron Microscopy (SEM). Figure 4 exhibits the SEM photographs of the surface and the cross section of the films. The white patches are the debris of the film during the sample preparation process. **Figure 4a** shows the surface photograph of the 50W:50G composite film, which was smooth and homogeneous, and these characteristics could be found in all the other samples (images not shown). **Figure 4b** exhibits the cross section of the single WPI film, where we observed that the network microstructure of the film was constituted with fine-stranded and twisted wormlike chains. These chains kept an interval of about 0.3 μm, and the diameter of one chain was about 1 μm. This observation was in accordance with the work of Clark et al. (*29*) and Langton and Hermansson (*30*). They mentioned that these chains were made up of β-sheets of the protein molecules. **Figure 4c** exhibits the cross section of the single gelatin film. To be distinguished from WPI, gelatin chains were nearly parallel-arranged, and larger intervals between the chains could be observed within the matrix. **Figure 4d** exhibits the cross section of the 50W:50G composite film, where the protein chains no longer had the typical fine-twisted or parallel-arranged conformations and these chains seemed to thicken caused by the blend of WPI and gelatin.

Mechanical Properties. Figure 5 shows the puncture strength and deformation versus WPI/gelatin mass ratio. The puncture strengths of the single WPI and gelatin film were very close, i.e. 48.0 ± 1.0 and 45.4 ± 2.7 N/mm, respectively. However, a minimum, i.e. 25.1 ± 1.5 N/mm, was found at 50W:50G. In contrast, the puncture deformation monotonically increased

from 5.8 to 12.5 mm when the mass ratio varied from 100W:0G to 0W:100G. The twisted network microstructure could improve the coupling strength of the WPI film and thus the puncture strength, but reduce the ductility (**Figure 4b**). If the integrity of such microstructure was destroyed by mixing with gelatin, the network microstructure became discontinuous (**Figure 4d**), and the puncture strength was thus reduced. The network microstructure with parallel-arranged long chains (**Figure 4c**) ensured the gelatin film having a certain mechanical strength (puncture strength and deformation). After mixing with WPI, the parallel-arranged characteristics were somewhat disordered and the deformation thus declined. The composite system could be depicted by a three-dimensional bond matrix constituted with the protein chains. For a given external strain, the bond sites were relaxed toward mechanical equilibrium with their neighbors by a systematic sequence of operations which steadily reduced the net residual force acting on each site (*31*). The matrix bonds were broken according to their local stress. Therefore, if the microstructure was discontinuous, the distribution of the force on each matrix bond became uneven, and led to a decline of the mechanical strength of the system. Cao et al. (*32*) also noticed that the mechanical properties of the gelatin alone were higher than those of the composite (type-B-bovine-bone gelatin/soy protein isolate) films. However, Denavi et al. (*12*) mentioned that the mix of the fish skin gelatin and soy protein isolate favored the increase of the puncture strength of the composite film (50S:50G and 25S:75G). The inconsistency was probably caused by the nature of the raw materials, but the mechanism was not clear yet. Moreover, the reviewer pointed out that the application of the different ASTM measurement methods could also cause different results as indicated in the work of Radebaugh et al. (*33*), where the puncture and tensile tests are compared.

Table 1. Thickness, Moisture Content (MC), Solubility (*S*), and WVP of Films Obtained with Different Proportions of WPI (W) and Gelatin (G)[a]

film	thickness (μm)	MC (%)	*S* (%)	WVP ($kg \cdot s^{-1} \cdot m^{-1} \cdot Pa^{-1}$)
100W:0G	96 ± 12 a	28.2 ± 1.0 a	19.5 ± 0.7 a	4.3 ± 0.1 a
75W:25G	95 ± 10 a	26.2 ± 1.2 b	22.5 ± 1.0 b	4.6 ± 0.1 b
50W:50G	93 ± 12 a	25.7 ± 1.1 b	25.1 ± 1.3 b	4.8 ± 0.2 bc
25W:75G	96 ± 8 a	25.6 ± 0.4 b	27.6 ± 0.9 c	4.9 ± 0.2 c
0W:100G	94 ± 12 a	23.7 ± 0.8 c	34.1 ± 2.4 d	5.3 ± 0.2 d

[a] Means in a column followed by different letters (a, b, or c) are significantly different among samples ($P < 0.05$).

Moisture Contents, Solubility Properties and Water Vapor Permeability. Table 1 shows the thickness, moisture content (MC), solubility (*S*) and water vapor permeability (WVP). The thickness of the films remained at about 95 μm in all cases ($P > 0.05$). MC of the single gelatin film was lower than that of the single WPI, but WVP and solubility were higher ($P < 0.05$). MC is a parameter related to the total void volume occupied by water molecules in the network microstructure of the film, the solubility related to the hydrophilicity of the materials and WVP related to the micropaths in the network microstructure. Among the composite films (75W:25G, 50W:50G and 25W:75G), MC had no significant variation ($P > 0.05$), which indicated that there was no significant variation of the total void volume during the mixing process. The structural characteristics of parallel-arranged and larger intervals (**Figure 4c**) made gelatin have continuous and run-through micropaths. These properties and high hydrophilicity enabled gelatin to increase WVP and solubility of the composite films.

Light Barrier Properties. Figure 6 showed the light transmittance of the films with the different WPI/gelatin mass ratio versus the wavelength, and the insert showed the enlarged UV region (200−300 nm). Within the UV region, the light transmittance of the single WPI film was lower than 0.1% caused primarily by the UV absorption of the tryptophan and tyrosine. With increasing the quantity of the gelatin, a protein lack of tryptophan (*34*), in the composite film, UV light transmittance increased progressively. Within the range of 400−800 nm, the visible light transmittances of the films were close or higher than 80%. The photos of the real films were exhibited in **Figure 7**.

Differential Scanning Calorimeter (DSC). Figure 8a shows the thermograms of the films with different WPI/gelatin mass ratios. The melting temperature (T_m) and enthalpy (ΔH) of each endothermic peak versus WPI/gelatin mass ratios are shown in **Figure 8b**. T_m of the single WPI film (100W:0G) was at 170.5 °C, which was in accordance with the data in the literature (*12*, *35*).

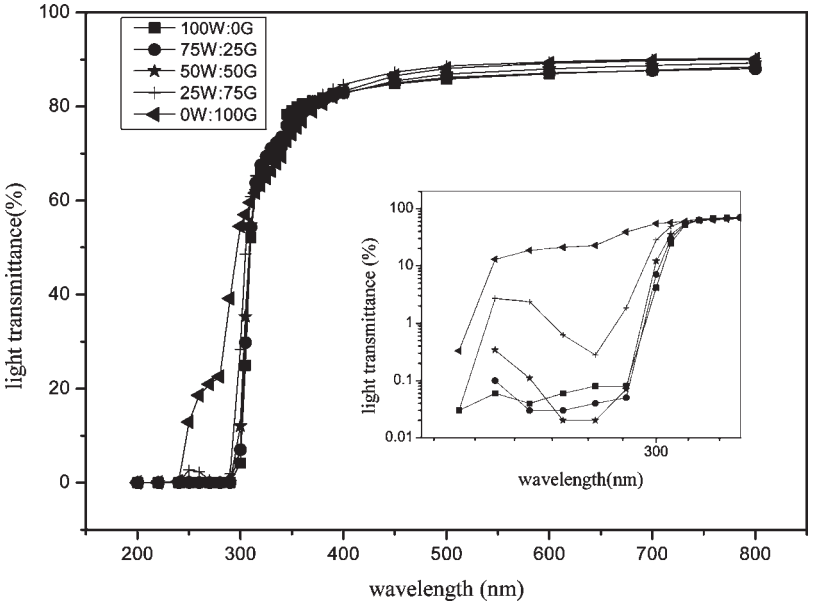

Figure 6. Light transmission of the films with different WPI/gelatin mass ratios versus the wavelength. The insert showed the enlarged UV region (200−300 nm).

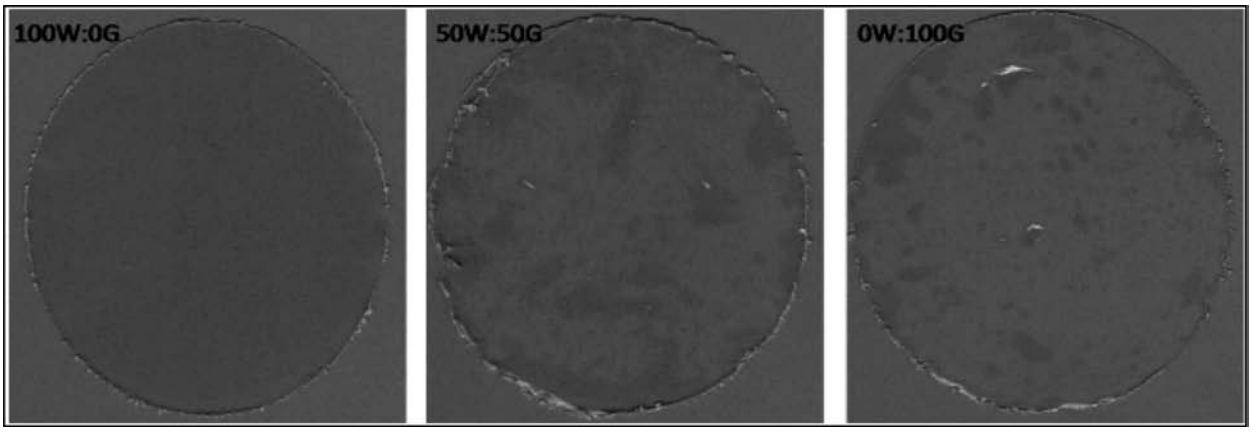

Figure 7. Photos of three film samples: single WPI film (100W:0G); composite film (50W:50G); single gelatin film (0W:100G).

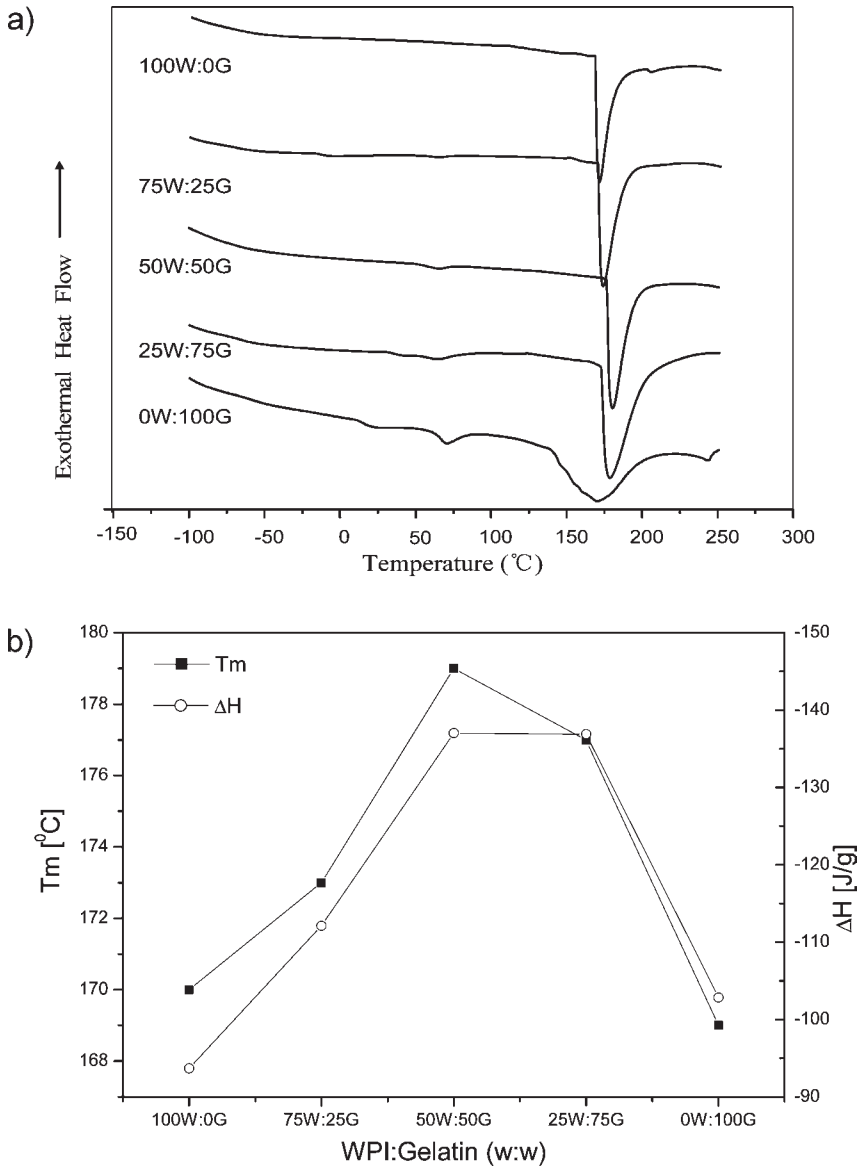

Figure 8. DSC thermograms of the films with different WPI/gelatin mass ratios versus the temperatures (**a**) and the variations of the melting temperature (T_m) and enthalpy (ΔH) of the WPI endothermic peaks versus WPI/gelatin mass ratios (**b**).

In the literature, T_m of gelatins varied greatly with the nature of the investigated material (*26*). In the present case, the single gelatin film (0W:100G) showed one broad melting peak at 169.1 °C and two weak peaks at about 20 and 70 °C. With increasing the gelatin content in the composite film, T_m of WPI film slightly increased and reached 179.1 °C at 50W:50G. Then, T_m decreased to the level of gelatin. In addition, the enthalpy increased also by 5% from 100W:0G to 50W:50G (**Figure 8b**). It was known that T_m

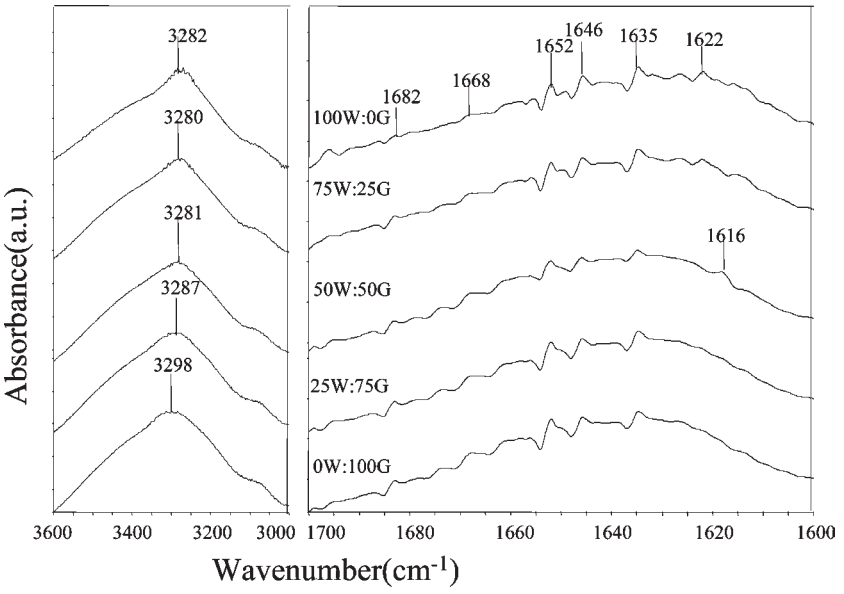

Figure 9. Deconvolution FT-IR spectra of the films.

was related to the heat-stability of the protein network structure, and proportional to the number and the strength of the cross-linkage of the network microstructure. Increasing of the melting temperature and enthalpy suggested that the composite film was reinforced by increasing the number and strength of the cross-linkage; indeed, we observed the thickening of the protein chains in **Figure 4d**. Meanwhile, we also observed a weak peak assigned to the gelatin occurring at 70 °C for the 50W:50G film. This peak indicated a discontinuous state, i.e. coexistence of WPI and gelatin phases, of the system mentioned in SEM measurements.

Fourier Transform Infrared Spectroscopy (FT-IR). Figure 9 compared the deconvoluted FT-IR spectra of the protein films with different WPI/gelatin mass ratios, and showed two spectral regions of interest: 3600−3000 and 1700−1600 (amide I). For the spectral region 3600−3000 cm^{-1}, strong bands were observed at 3282 (WPI) or 3298 cm^{-1} (gelatin) essentially due to −OH and NH stretching mode (**Figure 9**). At 50W:50G, the strong band shift to 3281 cm^{-1}, which was almost the same as WPI, but 17 cm^{-1} in the right of the gelatin. The displacement of the band suggested that cross-linking caused by hydrogen bonding occurred between amino or −OH group of the protein molecules (*36*). The shift of the strong band indicated that the hydrophilicity of gelatin was reduced, because the free −OH group of gelatin was involved more in hydrogen bonding association and was thus less susceptible to hydration (*36*).

Amide I absorption (1700−1600 cm^{-1}) is sensitive to the secondary structure of the protein and primarily represents the C═O stretching vibration of the amide group (*37*). In this region, several bands (1691, 1682, 1676, 1668, 1661, 1652, 1646, 1635, 1627 and 1616 cm^{-1}) were observed. A curve-fitting of the spectrum has been carried out using Lorentzian functions (**Figure 10**). The bands at 1661, 1652, and 1646 cm^{-1} could be attributed to α-helix/unordered segments, and the band at 1635 cm^{-1} was highly characteristic of amide groups involved in the extended β-sheet structure(*38*). The band at 1668 and 1676 cm^{-1} could be assigned to the turns. These six bands were rarely affected by the aggregation process (*39*, *40*). The bands at 1682 and 1622 cm^{-1} were due to the formation of intermolecular antiparallel β-sheets, and the position of the latter one could provide insights into the molecular structure of the aggregates (*40*). In the films, we observed that the band at 1622 cm^{-1} shifted to 1616 cm^{-1} at 50W:50G (**Figure 9**). A shift to a low wavenumber suggested the formation

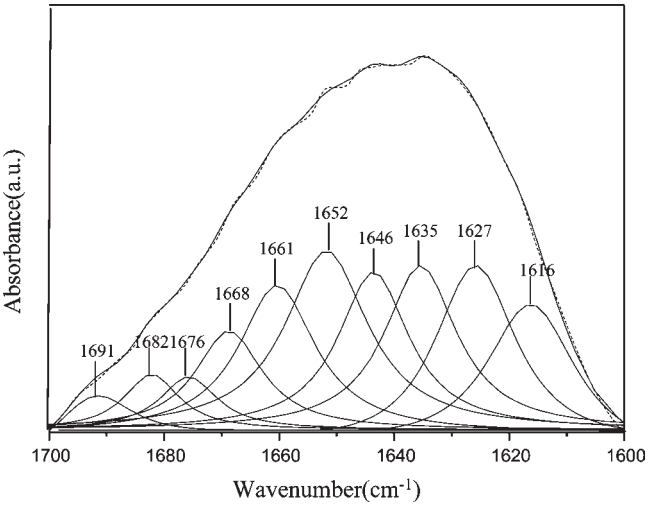

Figure 10. Curve-fitting of the spectrum for the 50W:50G composite film.

of fine-stranded aggregates caused by hydrogen bonds (*37*, *39*). The area of the aggregation bands at 1691, 1682, 1627, 1622, or 1616 cm^{-1} indicated that 35 ± 4% of the amide I was due to intermolecular β-sheet; therefore, it could be assessed that about 35% of the amino acids are engaged in β-sheet aggregation, whereas about 65% formed other structures such as α-helix, random coil segments and turns. The formation of intermolecular β-sheet is not unique to the present composite system and has been already observed in gels of some proteins like bovine serum albumin, glycinin, the major protein from soybeans or legumin, a globular protein from pea (*29*, *41*−*43*).

In conclusion, **Figure 11** schematically showed the network microstructure of the most typical protein systems based upon the results of the combination of the size, potential, IR, DSC and mechanical measurements etc. The size of the particles made by mixing the WPI and gelatin (particular 50W:50G) could be reduced by the electrostatic attraction and hydrogen bonding in water. After the treatment of the film-forming process, the single WPI chains were more twisted than gelatin. Through the electrostatic effects and hydrogen bonding, the chains formed in the mixing system could be thickened, and the discontinuous properties of the system became outstanding when WPI/gelatin mass

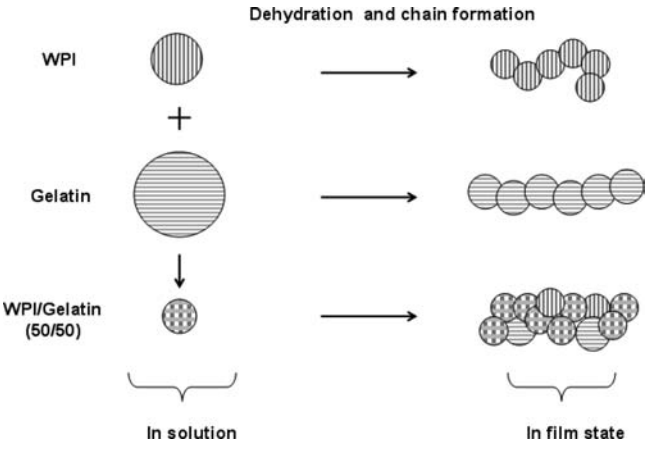

Figure 11. Comparison of the process of the film chain formation by protein aggregations in the single or mixed system. This figure is only schematic, where the particle form, mass ratio and size are not strictly complied with the real system.

ratio was close to 50W:50G. This discontinuity could lead to a decline of the puncture strength of the film.

ACKNOWLEDGMENT

Prof. Jingzhi Wei (Analysis Center, Tsinghua University, Beijing, China) and Prof. Yunjie Yan (Beijing National Center for Microscopy, Tsinghua University, Beijing, China) are acknowledged for their technical advice.

LITERATURE CITED

(1) Kester, J. J.; Fennema, O. Edible films and coating: A review. *Food Technol.* **1986**, *40*, 47–59.
(2) Stuchell, Y. M.; Krochta, J. M. Enzymatic treatments and thermal effects on edible soy protein films. *J. Food Sci.* **1994**, *59*, 1332–1337.
(3) Gontard, N.; Ring, S. Edible wheat gluten film: influence of water content on glass transition temperature. *J. Agric. Food Chem.* **1996**, *44*, 3474–3478.
(4) Krochta, J. M.; DeMulder-Johnston, C. Edible and biodegradable polymer films: challenges and opportunities. *Food Technol.* **1997**, *51*, 61–74.
(5) Anker, M.; Berntsen, J.; Hermansson, A. M.; Stading, M. Improved water vapor barrier of whey protein films by addition of an acetylated monoglyceride. *Innovative Food Sci. Emerging Technol.* **2002**, *3*, 81–92.
(6) Diaz-Sobac, A.; Garcia, H.; Beristain, C. I. Morphology and water vapour permeability of emulsion based on mesquite gum. *J. Food Process. Preserv.* **2002**, *26*, 141–144.
(7) Morillon, V.; Debeaufort, F.; Blond, G.; Capelle, M.; Voilley, A. Factors affecting the moisture permeability of lipid based edible films: A review. *Crit. Rev. Food Sci. Nutr.* **2002**, *42*, 67–89.
(8) Longares, A.; Monahan, F. J.; O'Riordan, E. D.; O'Sullivan, M. Physical properties of edible films made from mixtures of sodium caseinate and WPI. *Int. Dairy J.* **2005**, *15*, 1255–1260.
(9) Kim, S. J.; Ustunol, Z. Thermal properties, heat seal ability and seal attributes of whey protein isolate/lipid emulsion edible films. *J. Food Sci.* **2001**, *66*, 985–990.
(10) Wang, L. Z.; Liu, L.; Holmes, J.; Huang, J.; Kerry, J. F.; Kerry, J. P. Effect of pH and addition of corn oil on the properties of whey protein isolate-based films using response surface methodology. *Int. J. Food Sci. Technol.* **2008**, *43*, 787–796.
(11) Min, S. C.; Janjarasskul, T.; Krochta, J. M. Tensile and moisture barrier properties of whey protein-beeswax layered composite films. *J. Sci. Food Agric.* **2009**, *89*, 251–257.
(12) Denavi, G. A.; Pérez-Mateos, M.; Añón, M. C.; Montero, P.; Adriana, N.; Mauri, A. N.; Gómez-Guillén, M. C. Structural and functional properties of soy isolate and cod gelatin blend films. *Food Hydrocolloids* **2009**, *23*, 2094–2101.
(13) Zhou, J. J.; Wang, S. Y.; Gunasekaran, S. Preparation and characterization of whey protein film incorporated with TiO_2 nanoparticles. *J. Food Sci.* **2009**, *74*, 50–56.
(14) Pérez-Gago, M. B.; Krochta, J. M. Water vapor permeability of whey protein emulsion films as affected by pH. *J. Food Sci.* **1999**, *64*, 695–698.
(15) Simelane, S.; Ustunol, Z. Mechanical properties of heat-cured whey protein-based edible films compared with collagen casings under sausage manufacturing conditions. *J. Food Sci.* **2005**, *70*, E131–E134.
(16) McHugh, T. H.; Krochta, J. M. Sorbitol-vs glycerol-plasticized whey protein edible films: integrated oxygen permeability and tensile property evaluation. *J. Agric. Food Chem.* **1994**, *42*, 841–845.
(17) Banerjee, R.; Chen, H. Functional Properties of Edible Films Using Whey Protein Concentrate. *J. Dairy Sci.* **1995**, *78*, 1673–1683.
(18) Fang, Y.; Tungm, M. A.; Britt, I. J.; Yada, S.; Dalgleish, D. G. Tensile and barrier properties of edible films made from whey proteins. *J. Food Sci.* **2002**, *67*, 188–193.
(19) Arvanitoyannis, I. S.; Nakayama, A.; Aiba, S. Chitosan and gelatin based edible films: state diagrams, mechanical and permeation properties. *Carbohydr. Polym.* **1998**, *37*, 371–382.
(20) Gómez-Guillén, M. C.; Pérez-Mateos, M.; Gómez-Estaca, J.; López-Caballero, E.; Giménez, B.; Montero, P. Fish gelatin: a renewable material for developing active biodegradable films. *Trends Food Sci. Technol.* **2009**, *20*, 3–16.
(21) Kadler, K. E.; Holmes, D. F.; Trotter, J. A.; Chapman, J. A. Collagen fibril formation. *Biochem. J.* **1996**, *316*, 1–11.
(22) Hernàndez-Balada, E.; Taylor, M. M.; Phillips, J. G.; Marmer, W. N.; Brown, E. M. Properties of biopolymers produced by transglutaminase treatment of whey protein isolate and gelatin. *Bioresour. Technol.* **2009**, *100*, 3638–3643.
(23) Peleg, M. Characterization of the stress relaxation curves of solid foods. *J. Food Sci.* **1979**, *44*, 277–281.
(24) Osés, J.; Fabregat-Vázquez, M.; Pedroza-Islas, R.; Tomás, S. A.; Cruz-Orea, A.; Maté, J. I. Development and characterization of composite edible films based on whey protein isolate and mesquite gum. *J. Food Eng.* **2009**, *92*, 56–62.
(25) Gontard, N.; Guilbert, S.; Cuq, J. L. Edible wheat gluten films: Influence of the main process variables on film properties using response surface methodology. *J. Food Sci.* **1992**, *57*, 190–195.
(26) Sobral, P. J. A.; Menegalli, F. C.; Hubinger, M. D.; Roques, M. A. Mechanical, water vapor barrier and thermal properties of gelatin based edible films. *Food Hydrocolloids* **2001**, *15*, 423–432.
(27) Pérez-Mateos, M.; Montero, P.; Gómez-Guillén, M. C. Formulation and stability of biodegradable films made from cod gelatin and sunflower oil blends. *Food Hydrocolloids* **2009**, *23*, 53–61.
(28) Stading, M.; Hermansson, A. M. Viscoelastic behaviour of β-lactoglobulin structures. *Food Hydrocolloids* **1990**, *4*, 121–135.
(29) Clark, A. H.; Judge, F. J.; Richards, J. B.; Stubbs, J. M.; Suggett, A. Electron microscopy of network structures in thermally-induced globular protein gels. *Int. J. Pept. Protein Res.* **1981**, *17*, 380–392.
(30) Langton, M.; Hermansson, A. M. Fine-stranded and particulate gels of β-lactoglobulin and whey protein at varying pH. *Food Hydrocolloids* **1992**, *5*, 523–539.
(31) Termonia, Y. Tensile strength of discontinuous fibre-reinforced composites. *J. Mater. Sci.* **1990**, *25*, 4644–4653.
(32) Cao, N.; Fu, Y.; He, J. Preparation and physical properties of soy protein isolate and gelatin composite films. *Food Hydrocolloids* **2007**, *21*, 1153–1162.
(33) Radebaugh, G. W.; Murtha, J. L.; Julian, T. N.; Bondi, J. N. Methods for evaluating the puncture and shear properties of pharmaceutical polymeric films. *Int. J. Pharm.* **1988**, *45*, 39–46.
(34) Chiou, B.-S.; Avena-Bustillos, R. J.; Shey, J.; Yee, E.; Bechtel, P. J.; Imam, S. H.; Glenn, G. M.; Orts, W. J. Rheological and mechanical properties of cross-linked fish gelatins. *Polymer* **2006**, *47*, 6379–6386.
(35) Mauri, A. N.; Añõn, M. C. Effect of solution pH on solubility and some structural properties of soybean protein isolate films. *J. Sci. Food Agric.* **2006**, *86*, 1064–1072.
(36) Le Tien, C.; Letendre, M.; Ispas-Szabo, P.; Mateescu, M. A.; Delmas-Patterson, G.; Yu, H. L.; Lacroix, M. Development of Biodegradable Films from Whey Proteins by Cross-Linking and

Entrapment in Cellulose. *J. Agric. Food Chem.* **2000**, *48*, 5566–5575.

(37) Gilbert, V.; Rouabhia, M.; Wang, H.; Arnould, A.-L.; Remondetto, G.; Subirade, M. Characterization and evaluation of whey protein-based biofilms as substrates for in vitro cell cultures. *Biomaterials* **2005**, *26*, 7471–7480.

(38) Allain, A. F.; Paquin, P.; Subirade, M. Relationships between conformation of b-lactoglobulin in solution and gel states as revealed by attenuated total reflection Fourier transform infrared spectroscopy. *Int. J. Biol. Macromol.* **1999**, *26*, 337–344.

(39) Lefèvre, T.; Subirade, M. Molecular differences in the formation and structure of fine-stranded and particulate β-lactoglobulin gels. *Biopolymers* **2000**, *54*, 578–586.

(40) Lefèvre, T.; Subirade, M. Molecular, M. P. Description of the Formation and Structure of Plasticized Globular Protein Films. *Biomacromolecules* **2005**, *6*, 3209–3219.

(41) Nagano, T.; Mori, H.; Nishinari, K. Rheological properties and conformational states of β-conglycinin gels at acidic pH. *Biopolymers* **1994**, *34*, 293–298.

(42) Subirade, M.; Kelly, I.; Guéguen, J.; Pézolet, M. Molecular basis of film formation from a soybean protein: Comparison between the conformation of glycinin in aqueous solution and in films. *Int. J. Biol. Macromol.* **1998**, *23*, 241–249.

(43) Subirade, M.; Gueguen, J.; Pézolet, M. Conformational changes upon dissociation of a globular protein from pea: A Fourier transform infrared spectroscopy study. *Biochim. Biophys. Acta* **1994**, *1205*, 239–247.

Received for review November 20, 2009. Revised manuscript received March 25, 2010. Accepted March 25, 2010. This work was supported by China High-Tech (863) project (2007AA10Z311) and National Science and Technology Support Program (2006BAD27B04).